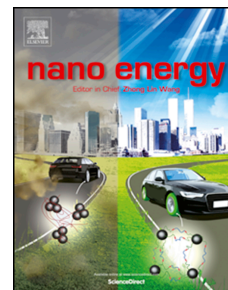


Journal Pre-proof

A long-lasting dual-function electrolyte additive for stable lithium metal batteries

Dongdong Wang, Haodong Liu, Mingqian Li, Dawei Xia, John Holoubek, Zhi Deng, Mingyu Yu, Jianhua Tian, Zhongqiang Shan, Shyue Ping Ong, Ping Liu, Zheng Chen



PII: S2211-2855(20)30446-8

DOI: <https://doi.org/10.1016/j.nanoen.2020.104889>

Reference: NANOEN 104889

To appear in: *Nano Energy*

Received Date: 14 January 2020

Revised Date: 23 April 2020

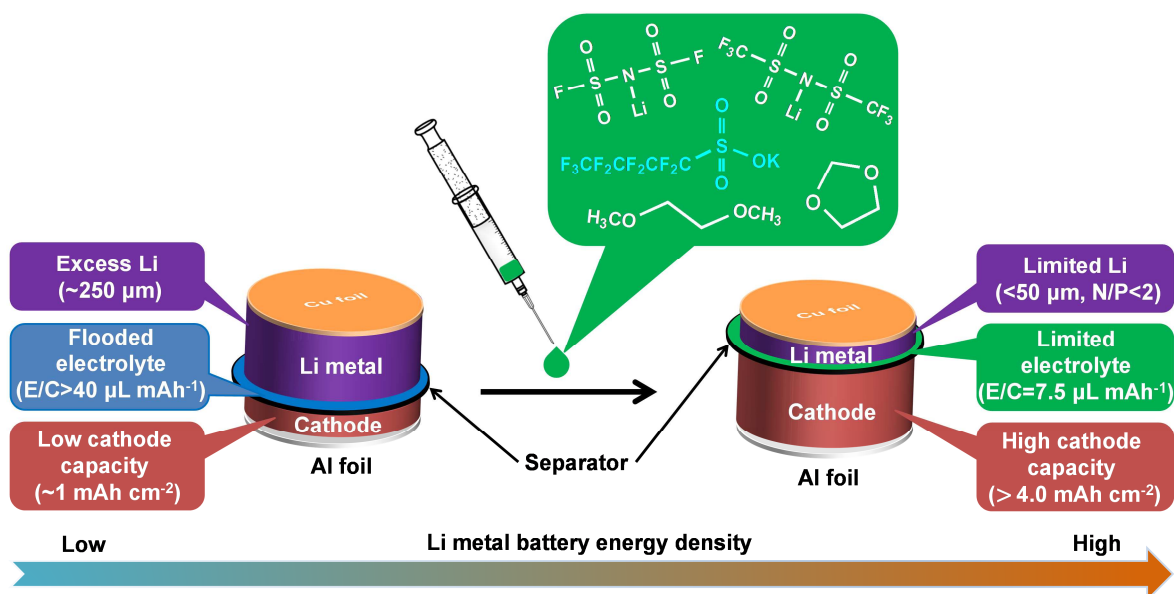
Accepted Date: 24 April 2020

Please cite this article as: D. Wang, H. Liu, M. Li, D. Xia, J. Holoubek, Z. Deng, M. Yu, J. Tian, Z. Shan, S.P. Ong, P. Liu, Z. Chen, A long-lasting dual-function electrolyte additive for stable lithium metal batteries, *Nano Energy* (2020), doi: <https://doi.org/10.1016/j.nanoen.2020.104889>.

This is a PDF file of an article that has undergone enhancements after acceptance, such as the addition of a cover page and metadata, and formatting for readability, but it is not yet the definitive version of record. This version will undergo additional copyediting, typesetting and review before it is published in its final form, but we are providing this version to give early visibility of the article. Please note that, during the production process, errors may be discovered which could affect the content, and all legal disclaimers that apply to the journal pertain.

© 2020 Published by Elsevier Ltd.

TOC Graphic



A Long-Lasting Dual-Function Electrolyte Additive for Stable Lithium Metal Batteries

*Dongdong Wang,^{a,b} Haodong Liu,^a Mingqian Li,^c Dawei Xia,^a John Holoubek,^a Zhi Deng,^a
Mingyu Yu,^a Jianhua Tian,^b Zhongqiang Shan,^b Shyue Ping Ong,^a Ping Liu^{a,c,d,e} and Zheng
Chen^{a,c,d,e*}*

^aDepartment of NanoEngineering, University of California San Diego, La Jolla, CA 92093

*^bSchool of Chemical Engineering and Technology, Tianjin University, Tianjin 300350, P. R.
China*

^cProgram of Chemical Engineering, University of California San Diego, La Jolla, CA 92093

*^dProgram of Materials Science and Engineering, University of California San Diego, La
Jolla, CA 92093*

*^eSustainable Power and Energy Center, University of California San Diego, La Jolla, CA,
92093, United States*

**Correspondence to: zhengchen@eng.ucsd.edu*

Abstract

Solid electrolyte interphases (SEI) plays a vital role in stabilizing lithium (Li) metal anodes for rechargeable batteries. However, forming robust SEI layers is challenging in the state-of-the-art electrolytes. Herein, we report a long-lasting and dual-function additive (potassium nonafluoro-1-butanesulfonate or KPBS) for dual-salt LiFSI-LiTFSI ether electrolyte. Our work suggests that the electrostatic shield effect from potassium ion (K^+) and the F-rich PBS^- anions with a middle lowest unoccupied molecular orbital (LUMO) level together promote the formation of a LiF-rich SEI during the Li plating/stripping process, which effectively restricts Li dendrite growth and suppresses electrolyte consumption. As a consequence, the designed electrolyte endows small nucleation overpotential, highly reversible Li plating/stripping, and excellent cycling stability. Specifically, with such an electrolyte, Li-Cu cells can maintain stable cycling during 400 cycles at 1 mA cm^{-2} for 1 mA h cm^{-2} with a high coulombic efficiency (CE) of 99.1%. Li-LiFePO₄ full cells displayed dramatically improved cycling stability after 100 cycles with high CE of 99.6% under relatively lean electrolyte condition ($7.5 \text{ } \mu\text{L mA h}^{-1}$), limited Li supply ($N/P = 1.2$) and high areal capacity (4.1 mA h cm^{-2}).

Keywords: potassium nonafluoro-1-butanesulfonate additive, solid electrolyte interphases, Li anodes, Li metal batteries, high areal capacity

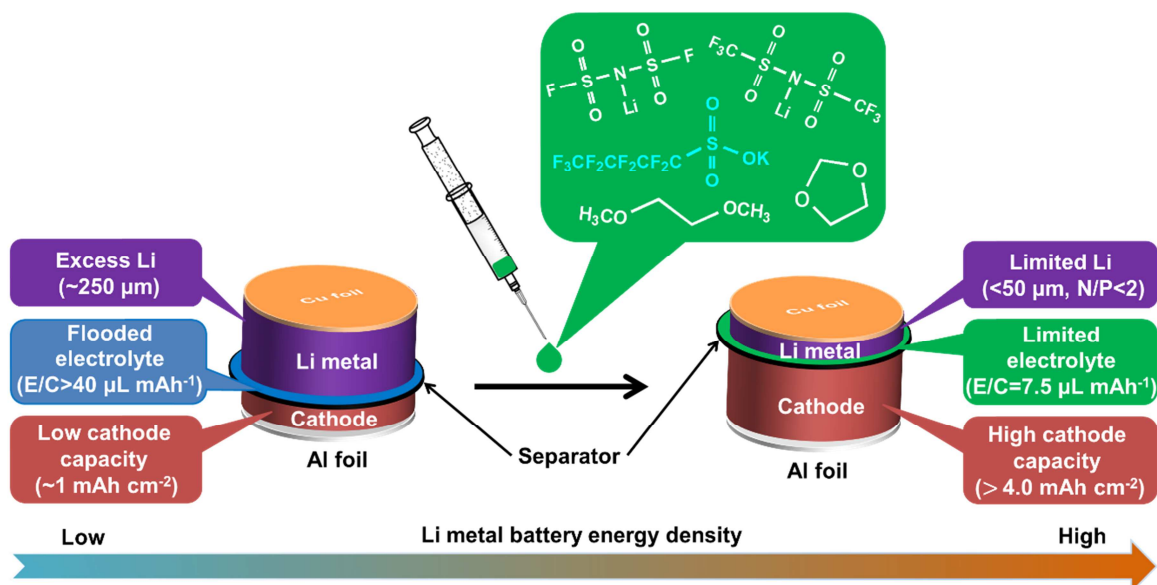
1. Introduction

The pursuit of high-energy density batteries for mobile devices and electrical vehicle has stimulated intensive research on new battery materials and systems.[1-3] Lithium (Li) metal is considered as one of the most promising anode materials, owing to its high theoretical specific capacity (3860 mA h g^{-1}), low density (0.534 g cm^{-3}), and low electrochemical potential (-3.040 V vs. the standard hydrogen electrode).[4-7] However, notorious issues with the formation of Li dendrites and insufficient coulombic efficiency (CE) during the plating/stripping process prevent its practical applications in rechargeable batteries.[8-10] These limitations are primarily attributed to fragile and inhomogeneous solid electrolyte interphases (SEI), which cause continuous consumption of fresh Li and electrolyte during cycling, leading to short battery life.[11, 12]

Of late, many efforts have been taken to enhance CE and suppress Li dendrite growth, including design of three-dimensional current collectors[13, 14], artificial SEI construction on the surface of Li,[15, 16] employment of solid-state electrolytes,[17] separator modification[18] and optimization of electrolyte compositions.[19] Among these methods, re-designing electrolytes is considered attractive for practical applications due to its facile commercial integration and cost effectiveness.[20] A significant advance of such electrolyte development is the transition from carbonate solvents to ethers, which possess better compatibility with Li metal anodes, exhibiting higher CE and better cycling performance owing to their reductive stability.[21, 22] Although long-cycling full cells have yet been demonstrated, some dual-salt electrolytes have shown better electrochemical performance than their single-salt counterparts presumably due to the formation of thinner and denser SEI.[4, 23-25] Dahn *et al.* recently reported a dual-salt LiDFOB-LiBF₄ electrolyte applied in the pouch cell and showed outstanding cycling performance with zero excess lithium under moderate pressure, superior to single-salt electrolytes.[24] Xu *et al.* reported a high concentration (4 M) dual-salt LiTFSI-LiDFOB electrolyte with better high-voltage cycling stability than single-salt ether electrolyte.[25] In both cases, the LiDFOB salt played critical role in improving cycling stability after its decomposition, in spite of their different SEI compositions. It was also commonly found that adding a small amount of additives (*e.g.*,

LiNO₃) into ether electrolyte can enhance the CE of Li metal anodes, however the cycling stability still requires further improvement owing to the consumption of additives during each charge discharge cycle.[26-28] Earlier studies also suggest that the formation of a LiF-containing layer is a key to achieving high CE and long cycle life for Li metal anodes as LiF has low reactivity and good Li⁺ conductivity.[29-31] Therefore, efforts have been focused on designing novel electrolytes, which *in-situ* constructs LiF-containing SEI during cycling to suppress Li dendrite formation and enhance CE of Li metal anodes. However, many works employing such electrolyte design criterion reported Li metal full cells with impractically low areal loadings of cathode active material (< 10 mg cm⁻²), large excess of Li supply (thickness > 50-250 μm) and flooded electrolytes (the electrolyte-to-capacity ratio was typically above 40 μL mA h⁻¹), limiting the energy density of the Li metal battery (Scheme 1).[32-35]

Herein, we report a novel electrolyte additive (potassium nonafluoro-1-butananesulfonate or KPBS) for Li metal batteries. We developed a hybrid ether electrolyte by adding 0.02 M KPBS into the dual-salt LiFSI-LiTFSI system to stabilize Li metal anodes under full cell conditions. The KPBS additive serves two functions: promoting uniform Li deposition via an electrostatic shield mechanism and tuning the SEI composition. Compared to the LiFSI-LiTFSI electrolyte, a stable and robust LiF-rich SEI layer was formed in KPBS-LiFSI-LiTFSI electrolyte, which effectively minimizes electrolyte decomposition and restricts dendrite growth. In addition, the K⁺ ions present in the electrolyte are not consumed during cycling, representing a great advantage over other reported additives. As a result, the cycling stability of Li-Cu cells was enhanced from 200 cycles to 400 cycles at current density of 1 mA cm⁻² for 1 mA h cm⁻² with a higher average CE of 99.1%. The Li-LFP full cells containing the KPBS electrolyte additive showed an improved cycling stability of 400 cycles with a high areal capacity of 4.1 mA h cm⁻² in sharp contrast to the pristine LiFSI-LiTFSI electrolyte, which exhibited significant degradation under the same conditions. Furthermore, stable cycling (100 cycles) and high CE (99.6%) of Li-LFP full cells was obtained under relatively lean electrolyte condition (7.5 μL mA h⁻¹), with limited Li supply (N/P = 1.2) and high areal capacity (4.1 mA h cm⁻²) (**Scheme 1**).



Scheme 1 A schematic illustration of applying the KPBS-LiFSI-LiTFSI electrolyte to achieve high energy density for Li metal battery with limited N/P ratio, relatively lean electrolyte and high mass loading.

2. Experimental Section

2.1. Electrolyte preparation: Lithium bis(trifluoromethanesulfonyl)imide (LiTFSI, 99.9%), lithium bis(fluorosulfonyl)imide (LiFSI, 99.9%), 1,3-dioxolane (DOL, 99.5%), 1,2-dimethoxyethane (DME, 99.5%), potassium perfluorobutane sulfonate (KPBS) and lithium perfluorobutane sulfonate (LPBS) were all purchased from Sigma-Aldrich. The dual-salt electrolyte was selected as the baseline (LiFSI-LiTFSI), which consisted of 1 M LiTFSI and 1 M LiFSI with DOL/DME (molar ratio = 1:4). As a comparison, KPBS was added into LiFSI-LiTFSI electrolyte (KPBS-LiFSI-LiTFSI) with different concentration (0.01 M, 0.02 M and 0.03 M). LPBS was added into LiFSI-LiTFSI electrolyte (LPBS-LiFSI-LiTFSI) with a concentration of 0.02 M. All electrolytes were prepared in an argon-filled glove box.

2.2. Cell Preparation and Electrochemical Measurements: The cathodes were prepared based on the following procedure: LiFePO₄ (LFP), super-P and polyvinylidenedifluoride (PVDF) were uniformly dispersed in N-methyl 2-pyrrolidone (NMP) in a weight ratio of 80:10:10. The well-mixed slurry was cast onto Al foil using a doctor blade. The cast

electrodes were dried under vacuum at 120 °C for 8 h. The areal mass loading of the active material was 25 mg cm⁻². 2032-type coin cells were used for all the electrochemical testing in this work. The Celgard 25 µm trilayer polypropylene (PP)-polyethylene (PE)-PP membrane was used as the separator. The asymmetric Li-Cu cells were galvanostatically tested at a current density of 1.0 and 2.0 mA cm⁻² using Neware BTS Tester. In each cycle, metallic Li was deposited onto Cu substrate for one hour during charging then the cells were discharged to the cutoff voltage of 1.0 V (vs. Li⁺/Li) at the same current. The symmetric Li-Li cells were galvanostatically cycled at different current densities (2.0, 4.0 mA cm⁻²) with time-controlled charge and discharge cycles. Li-LFP full cells were assembled using Li foil (500 µm) as the counter electrode and LFP as the cathode. Li-LFP full cells were assembled using Li deposited Cu as the working electrode [negative/positive ratio (N/P) = 0, 1.2 and 2.4] and LFP as the cathode. All Li-LFP full cells were galvanostatically cycled over a voltage range of 2.5-3.8 V at room temperature. Electrochemical impedance spectroscopy (EIS) measurement of cells after different cycles was executed by using a Metrohm Autolab potentiostat in a frequency range of 0.1-10⁵ Hz and with a voltage perturbation of 5 mV.

2.3. Physical Characterizations: The morphology and thickness of the deposited Li metal film, X-ray spectroscopy (EDX) analysis and elemental mapping of SEI films were determined using scanning electron microscope (FEI Quanta 250 SEM). The samples were adhered to a double-sided carbon tape and placed on a specimen holder. The prepared samples were sealed in a laminated plastic bag inside the glovebox for transferring to the SEM. X-ray photoelectron spectroscopy (XPS) was performed using a Thermo Fisher Scientific Model K-Alpha spectrometer equipped with Al K α radiation (1486.6 eV). The relative elemental ratios of Li, F, C, O, S and N were calculated from the peak areas in the XPS spectra using the following equation:

$$\text{Atomic concentration (\%)} = \frac{A_x / \text{RSF}_x}{\sum(A_i / \text{RSF}_i)}$$

where A is the intensity of the relative element and RSF is the atomic sensitivity factor of the corresponding peak.

2.4. *Density Functional Theory (DFT) Calculations:* The HOMO and LUMO energy level of each molecular component in the electrolyte was estimated from the ionization potential (IP) and electron affinity (EA), respectively, using the following equations:

$$\varepsilon_{\text{HOMO}} = -\text{IP} = E(\text{mol}) - E(\text{mol}_{\text{ox}}),$$

$$\varepsilon_{\text{LUMO}} = -\text{EA} = E(\text{mol}_{\text{red}}) - E(\text{mol}),$$

where $E(\text{mol})$, $E(\text{mol}_{\text{ox}})$ and $E(\text{mol}_{\text{red}})$ refer to the energy of molecule itself, oxidized molecule with one electron removed and reduced molecule with one electron added, respectively. The adiabatic EA/IP approach was adopted, where the geometry of molecule after removing/adding an electron was also optimized. All calculations were performed using the Gaussian 09 quantum chemistry package.[36] The hybrid B3LYP density functional based on Becke's three-parameter exchange functional[37] and the correlation functional of Lee, Yang, and Parr were chosen for all calculations.[38] Geometry optimizations were carried out at the B3LYP/6-31+G(d) level, followed by single-point energy calculations at the B3LYP/6-311+G(2d,p) level. The inclusion of diffuse functions in the basis sets ensures an adequate description of the diffuse electron cloud of anions.

3. Results and Discussion

3.1 Asymmetric Li-Cu Cells

In order to evaluate the Li metal cyclability of the systems of interest, asymmetric cells consisting of Cu foil working electrodes and Li metal counter electrodes were assembled employing the same volume of LiFSI-LiTFSI and KPBS-LiFSI-LiTFSI electrolytes. Firstly, the change of open-circuit voltage (OCV) was monitored over time. Since OCV refers to the potential difference between two electrodes, the decline of OCV may indicate galvanic corrosion of the Li metal, which consequently reflects the chemically vulnerable nature of the electrolyte.[39, 40] As shown in **Figure 1A**, the cell employing the KPBS-LiFSI-LiTFSI electrolyte exhibited a more stable voltage curve without obvious voltage drops compared to that with the LiFSI-LiTFSI electrolyte, demonstrating a better chemical stability. To confirm this, the morphology of Li metal rested in different electrolytes for 80 h was examined by scanning electron microscopic (SEM) imaging. As shown in **Figure S1**, a significant amount

of pores and high surface roughness are obtained on the surface of Li metal in LiFSI-LiTFSI electrolyte comparing to that in KPBS-LiFSI-LiTFSI electrolyte, indicating more severe galvanic corrosion of Li metal in the former electrolyte.

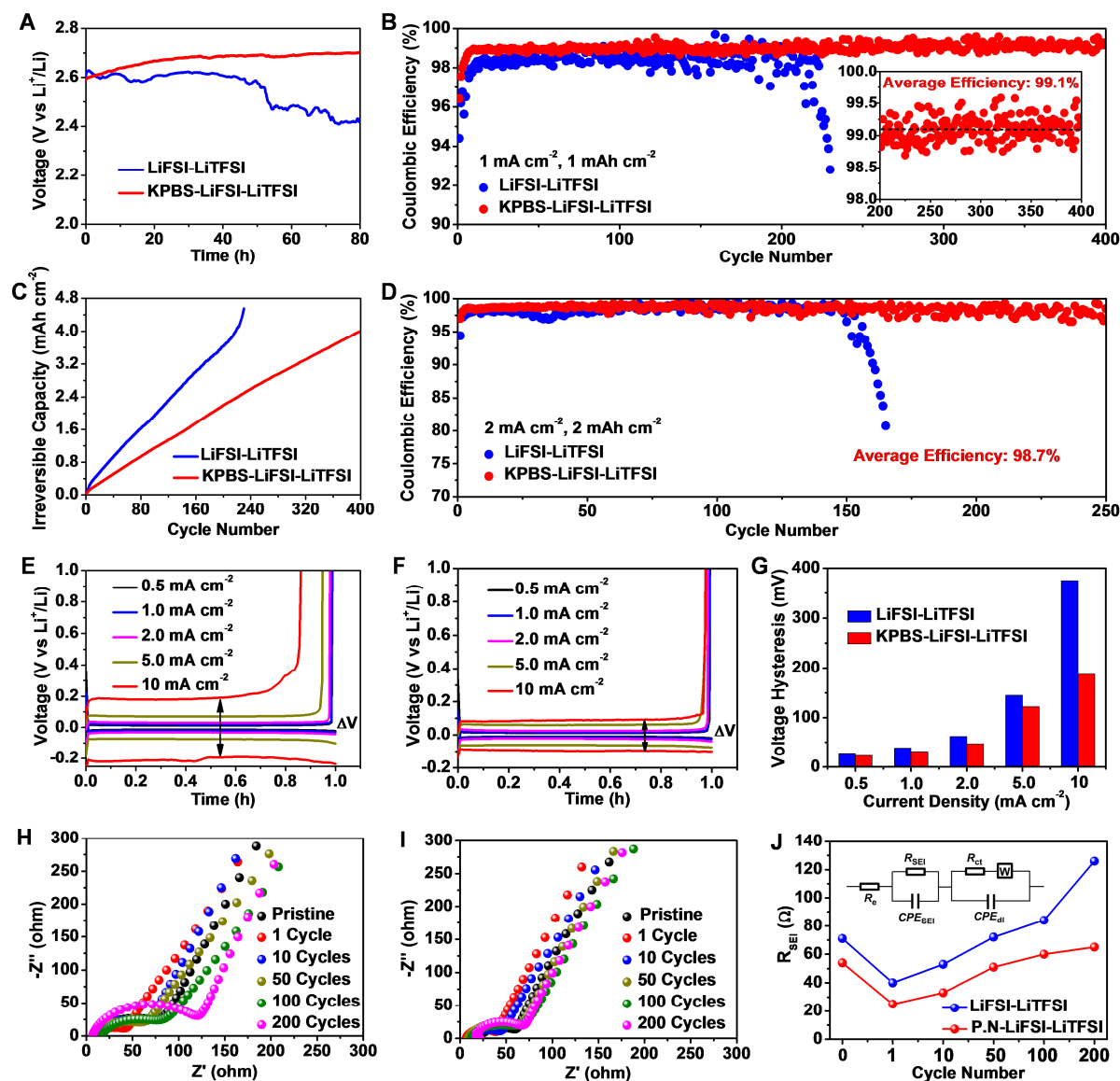


Figure 1 The electrochemical performance of Li-Cu cells. (A) Changes of OCV with Li-Cu cells over time with different electrolytes; (B) CE of Li-Cu cells with different electrolytes at current density of 1 mA cm⁻²; (C) The accumulated irreversible capacity of Li-Cu cells upon cycling with different electrolytes; (D) CE of Li-Cu cells with different electrolytes at a current density of 2 mA cm⁻²; the Li plating and stripping voltage profiles at different current densities with (E) LiFSI-LiTFSI and (F) KPBS-LiFSI-LiTFSI electrolyte; (G) Voltage hysteresis at different current densities; (H) Nyquist plots of LiFSI-LiTFSI electrolyte at different cycle numbers; (I) Nyquist plots of KPBS-LiFSI-LiTFSI electrolyte at different cycle numbers; (J) R_{SEI} vs Cycle Number.

(G) Summarized overpotential of the Li-Cu cells with different electrolytes at various current densities. Nyquist plots of the Li-Cu cells at different cycles with various electrolytes (H) LiFSI-LiTFSI, (I) KPBS-LiFSI-LiTFSI; (J) The fitted interfacial resistance of Li-Cu cells with different electrolytes at various cycles. The inset in (J) is equivalent circuit adopted to fit the Nyquist plots.

The CE of Li-Cu cells with three different baseline electrolytes were tested (2M LiTFSI, 2M LiFSI and 1M LiFSI+1M LiTFSI). As shown in **Figure S2**, Li-Cu cells with the LiFSI-LiTFSI electrolyte showed the most stable cycling stability among the three baseline electrolytes, indicating the positive effect of the dual salt, which in agreement with the previous reports,[23, 41, 42] The main reason could be ascribed to the role of mixed anions in regulating the Li nucleation, SEI chemistry, and surface morphology. Thus, the dual salt electrolyte was selected as the control system for the addition of KPBS. **Figure 1B** exhibits the CE of such additive systems at 1 mA cm^{-2} for 1 mA h cm^{-2} . It was observed that CE of LiFSI-LiTFSI cell reached 94.4% in the first cycle, which then increased to and stabilized at 98.5% in the first 130 cycles, which began to fluctuate and then declined rapidly with more cycles. The average CE of the LiFSI-LiTFSI cell was 98.3% from 1 to 230 cycles, corresponding to an accumulated irreversible capacity of 4.6 mA h cm^{-2} after 230 cycles (**Figure 1C**). By contrast, the KPBS-LiFSI-LiTFSI cell exhibited an initial CE of 96.4%, then increased quickly to $\sim 99\%$ and remained stable over 400 cycles. This data corresponds to an average CE of 99.1% (**Figure 1B**, inset), and an accumulated irreversible capacity of only 2.5 mA h cm^{-2} after 230 cycles (**Figure 1C**). This improvement in CE and cycling stability with the KPBS additive is even more pronounced at higher current densities and capacities; CE at 2 mA cm^{-2} and 2 mA h cm^{-2} show that the LiFSI-LiTFSI cell exhibited a sharp decline in CE after 150 cycles, while the KPBS-LiFSI-LiTFSI cell displayed stable cycling for 250 cycles with higher average CE at 98.7% (**Figure 1D**).

The Li plating and stripping overpotential at various current densities was also investigated, where the voltage profiles of such studies are found in **Figure 1E** and **1F**. The average CE was 98.8%, 98.5%, 97.8%, 94.8% and 86.1% at 0.5, 1, 2, 5 and 10 mA cm^{-2} ,

respectively. For KPBS-LiFSI-LiTFSI cell, the average CE was 99.2%, 99.1%, 98.7%, 97.8% and 97.5% at 0.5, 1, 2, 5 and 10 mA cm⁻², respectively, which is higher than that of the LiFSI-LiTFSI cell, especially at high rates (**Figure S3**). The voltage gap between the charge and discharge plateaus reflects the degree of overpotential of the Li-Cu cells with the different electrolytes. As summarized in **Figure 1G**, the overpotential of KPBS-LiFSI-LiTFSI cell was found to be 23, 31, 47, 122 and 187 mV at 0.5, 1, 2, 5 and 10 mA cm⁻², respectively, consistently lower than that 28, 39, 62, 145 and 376 mV of the LiFSI-LiTFSI cell at 0.5, 1, 2, 5 and 10 mA cm⁻², respectively, further suggesting the positive role of KPBS additive.

In order to study the interfacial characteristics of the Li-Cu cells, electrochemical impedance spectrum (EIS) measurements were carried out. **Figure 1H** and **1I** show the Nyquist plots of the Li-Cu cells with the LiFSI-LiTFSI and KPBS-LiFSI-LiTFSI electrolytes after 1, 10, 50, 100 and 200 cycles at 1.0 mA cm⁻² for 1.0 mA h cm⁻², respectively. The shapes of all Nyquist plots are similar, consisting of a small intersection and a depressed semicircle in the high frequency followed by a quasi-straight line. In general, the high frequency semicircle can be ascribed to surface film resistance (R_{SEI}) of the Li anode, where a modified Randle-Ershler equivalent circuit model (**Figure 1J, inset**) was used to fit the Nyquist profile for a quantitative understanding of the electrolyte interfaces.[43, 44] Before cycling, the KPBS-LiFSI-LiTFSI cell displayed a lower R_{SEI} than the LiFSI-LiTFSI cell. After the first cycle, the R_{SEI} of two cells both decreased likely owing to the formation of SEI under bias. As the charge/discharge process continued, the R_{SEI} of LiFSI-LiTFSI cell increased quickly during the cycling process, while the R_{SEI} of KPBS-LiFSI-LiTFSI cell increased slowly, implying a thinner and more robust SEI. These trends are summarized in **Figure 1J**, which compares the change of R_{SEI} of cells with different electrolytes after different cycles.

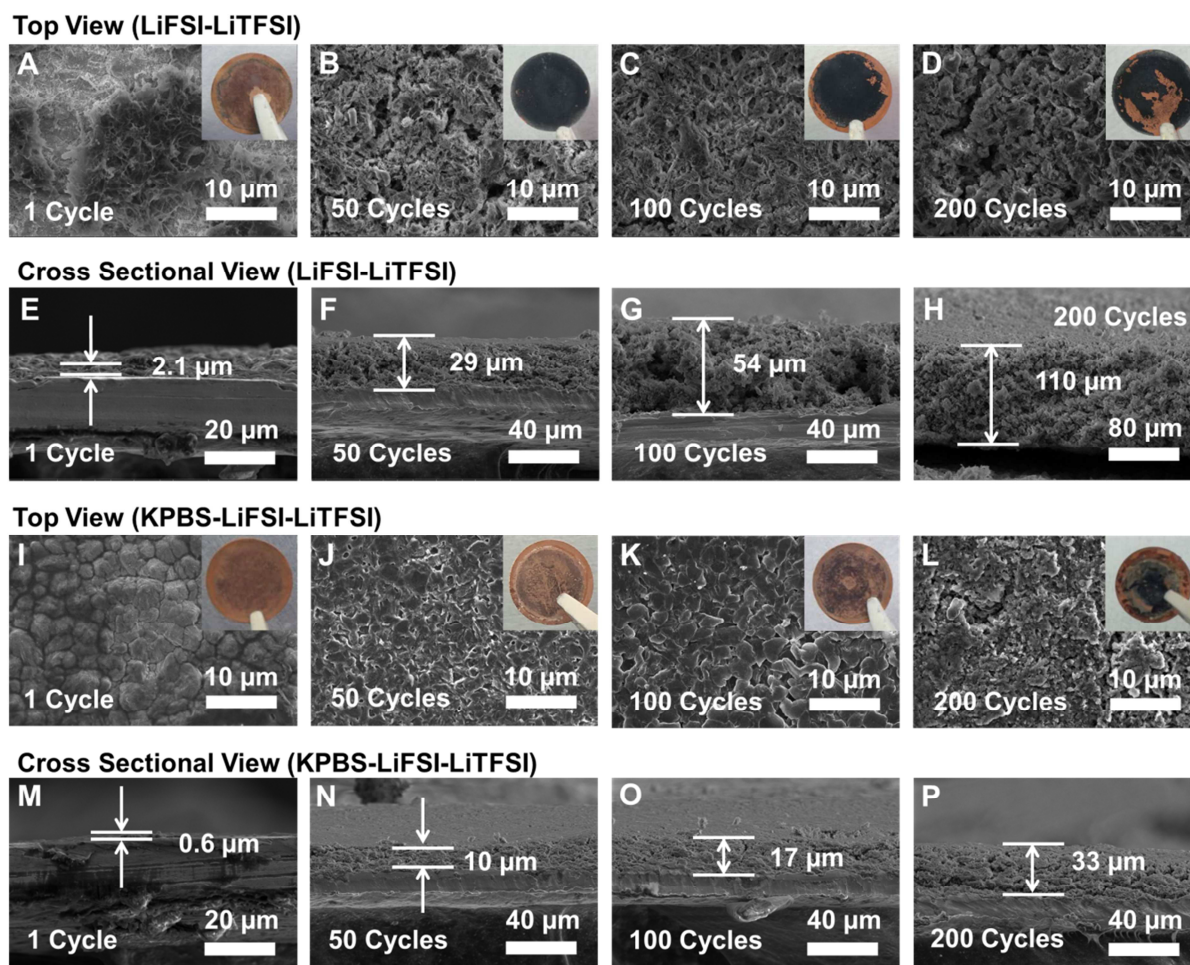


Figure 2 Investigation of morphology on cycled Li metals. SEM images of SEI morphology of Li-Cu cells under stripped condition with different electrolytes after different cycles: top view of LiFSI-LiTFSI cell after (A) 1 cycle, (B) 50 cycles, (C) 100 cycles, (D) 200 cycles; the cross-sectional view of LiFSI-LiTFSI cell after (E) 1 cycle, (F) 50 cycles, (G) 100 cycles, (H) 200 cycles; top view of KPBS-LiFSI-LiTFSI cell after (I) 1 cycle, (J) 50 cycles, (K) 100 cycles, (L) 200 cycles; the cross-sectional view of KPBS-LiFSI-LiTFSI cell after (M) 1 cycle, (N) 50 cycles, (O) 100 cycles, (P) 200 cycles; Each inset is a digital photo of the electrode taken after the cells had been disassembled.

To support the observed electrochemical performance, the SEI and dead Li morphology and thickness evolutions of Li-Cu cells with two electrolytes were examined after the first, 50th, 100th and 200th cycle under a stripped condition (**Figure 2**). For the LiFSI-LiTFSI cell, the SEI appeared porous and uneven with some Li fibers distributed on the Cu surface after

the first cycle (**Figure 2A**). From the cross-sectional view, the thickness of the SEI was measured to be 2.1 μm (**Figure 2E**). As the cycle number increased (50 and 100 cycles), a thicker SEI with looser and porous structure was formed (**Figure 2B, C**). The thickness of the SEI layer increased to 29 μm and 54 μm , respectively, owing to the decomposition of the electrolyte (**Figure 2F, G**). After 200 cycles, the SEI was found to be partially delaminated from the Cu foil due to the inhomogeneous and loose structures with large thickness (110 μm), which is generally associated with dead Li (**Figure 2D, H**).^[30] By contrast, the KPBS-LiFSI-LiTFSI cell exhibited a very thin and smooth film on the Cu foil after the first cycle (**Figure 2I, M**). After the 50 and 100 cycles, a dense and uniform SEI was formed on the Cu foil (**Figure 2J, K**). At these cycles, the thickness of the SEI was estimated to be only 10 μm and 17 μm , respectively, which suggests reduced electrolyte consumption (**Figure 2N, O**). Even after 200 cycles, SEI still remained stable and no clear dendritic dead Li can be observed (**Figure 2L**), which is also evident in the thin cross section of ~ 33 μm displayed in **Figure 2P**. The SEI morphology of plated Li metals under various current densities can be found in **Figure S4**. These results are consistent with the EIS results and irreversible capacity measurements, confirming the effectiveness of KPBS for the suppression of electrolyte decomposition and uniform Li deposition.

To identify the composition of the SEI layers, X-ray photoelectron spectroscopy (XPS) measurement was performed on the cycled Cu foils in different electrolytes after various cycles. As shown in the F1s spectra, the peaks at 688.5 and 684.4 eV are attributed to $\text{SO}_2\text{-F/C-F}$ and LiF, respectively (**Figure 3A**).^[45] At all measured cycles, the SEI from the KPBS-LiFSI-LiTFSI electrolyte exhibited a significantly higher LiF content than that produced by the LiFSI-LiTFSI electrolyte. Although the LiF content decreased as the cycle number increased, LiF was still the main component in SEI from the KPBS-LiFSI-LiTFSI electrolyte, which likely contributes to the more rigid and stable SEI observed. These results are also confirmed by Li 1s spectra, where the peaks at 57.0 and 54.4 eV can be assigned to LiF and $\text{Li}_2\text{O/Li}_x\text{S}$, respectively (**Figure 3B**).^[46-48] **Figure S5** shows the S 2p XPS spectra of SEI films from two electrolytes after different cycles, where the peaks at 170.8, 168.5 and 163-164.7 eV belongs to $\text{Li}_2\text{S}_2\text{O}_4$, Li_2SO_3 and Li_xS groups, respectively.^[49] In the O 1s

spectra (**Figure S6**), four peaks can be assigned to $-O-C=O$ (534.5 eV), C-O (533.8 eV), $-SO_2$ (532.6 eV) and Li_2O (529.5 eV), respectively.[50] The C1s spectra of the SEI in different electrolytes after different cycles were also examined, where the organic products can be attributed to C-F (291.5 eV), C-O (286.1 eV) and C-C/C-H (284.8 eV) bonds, respectively (**Figure S7**).[51] Through O 1s and C 1s spectra, the smaller accumulation of C and O elements of SEI in the KPBS-LiFSI-LiTFSI electrolyte suggests that the KPBS can alleviate the reductive decomposition of organic solvent. The N 1s spectra showed an obvious peak at 399.7 eV, which corresponds to the N-S groups of LiTFSI and LiFSI before cycling. An additional peak at 396 eV was observed after 200 cycles, which can be attributed to the Li_3N group (**Figure S8**).[28]

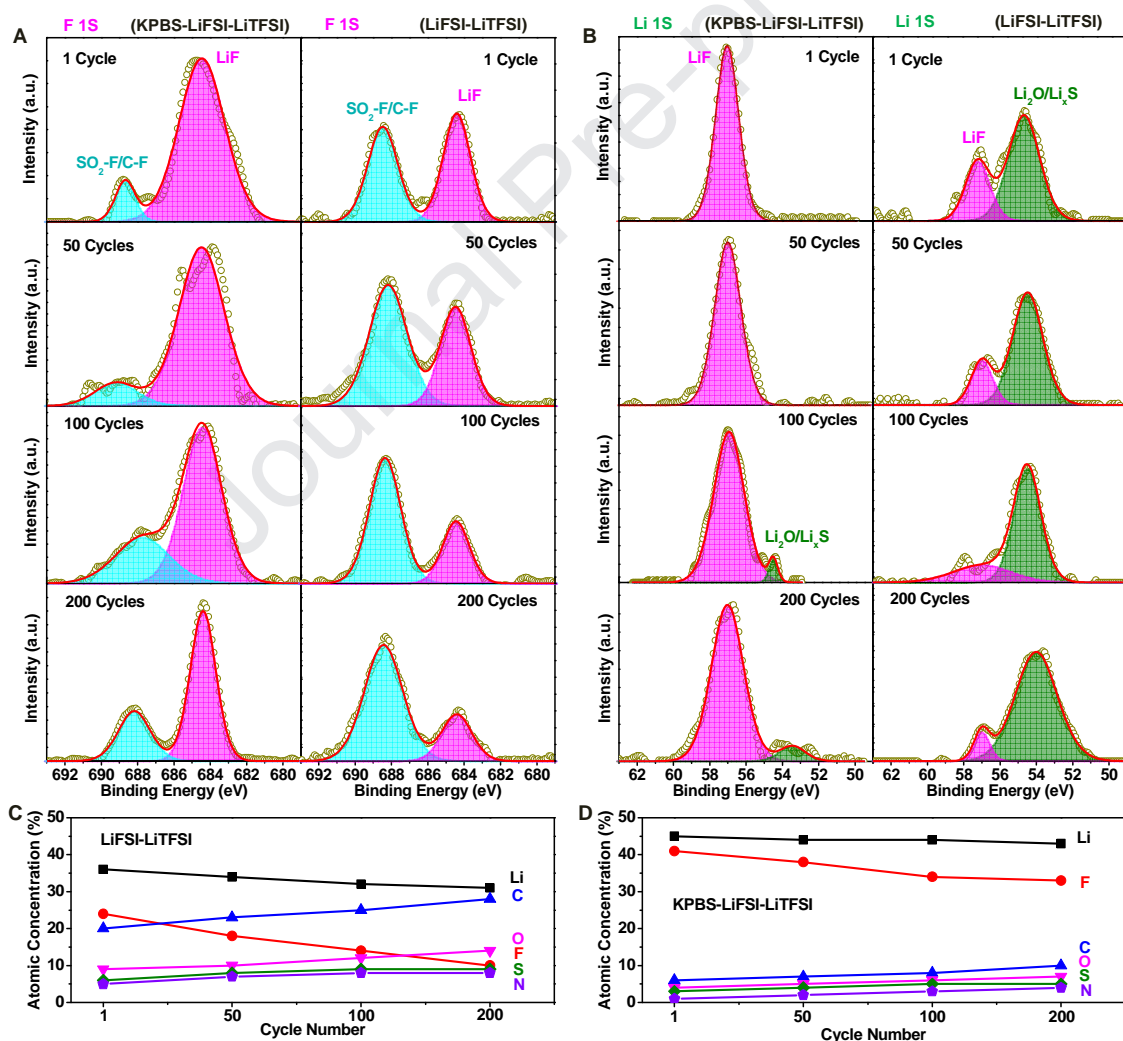


Figure 3 Investigation of SEI compositions on the cycled Li-metals. (A) XPS spectra of F 1s for SEI films in different electrolytes at various cycles; (B) XPS spectra of Li 1s for SEI

films in different electrolytes at various cycles; Composition evolution of SEI layers in different electrolytes after various cycles in (C) LiFSI-LiTFSI and (D) KPBS-LiFSI-LiTFSI electrolyte.

Using the aforementioned spectra, the relative elemental ratios of Li, F, C, O, S and N were calculated to elucidate the evolution of SEI composition with cycling. As cycle number progressed in SEI from the LiFSI-LiTFSI electrolyte, the content of LiF decreased sharply while the increase of the C and O content is likely due to the massive decomposition of organic solvent (**Figure 3C**). However, in the SEI from the KPBS-LiFSI-LiTFSI electrolyte, there was inevitable decomposition of ether solvent during the cycling process, but LiF-rich SEI can be still obtained even after 200 cycles (**Figure 3D**). The advantages of such LiF-rich SEI for improved CE mainly lie in three aspects: (1) LiF is known as a good electron insulator and can effectively eliminate electron leakage through the interphase, which prevents sustained electrolyte decomposition and dendrite formation; (2) LiF has much higher interfacial energy to Li metal than other Li compounds (e.g., Li_2O , Li_xS), and hence accelerates Li transport along the interface, directing a uniform Li deposited morphology; [52, 53] (3) LiF films with large surface energy are more resistant to fracture, which explains the better mechanical and morphological stability of Li metal anodes with LiF protection during Li deposition and volume expansion process. [54]

3.2 Symmetric Li-Li Cells

Symmetric Li-Li cells were also assembled to further confirm the cycling stability of the KPBS-LiFSI-LiTFSI electrolyte. **Figure 4A** shows the Li plating/stripping cycling at a constant current of 2 mA cm^{-2} with a capacity of 2 mA h cm^{-2} for the two electrolytes. The voltage fluctuation of Li-Li cell with the KPBS-LiFSI-LiTFSI electrolyte decreased in the initial 80 h, and then remained stable without any overpotential increase in the following 1000 h. In contrast, Li-Li cell with the LiFSI-LiTFSI electrolyte indicated a significant impedance increase after 300 h, where the overpotential increased to over five times higher than that of cell with the KPBS-LiFSI-LiTFSI electrolyte after 600 h. A detailed comparison of voltage profiles between 300 and 310 h is also shown in **Figure 4B**, where the overpotential of the KPBS-LiFSI-LiTFSI cell was 35 mV, much lower than that of the

LiFSI-LiTFSI cell (65 mV). Li plating/stripping cycling of two electrolytes was also conducted at a higher current density of 4 mA cm^{-2} with a capacity of 2 mA h cm^{-2} (**Figure 4C, D**). Similarly, the KPBS-LiFSI-LiTFSI cell displayed a longer cycling life and lower overpotential than the LiFSI-LiTFSI cell, further demonstrating the formation of a more stable SEI film which can minimize the consumption of electrolytes and inhibit Li metal dendrite growth.

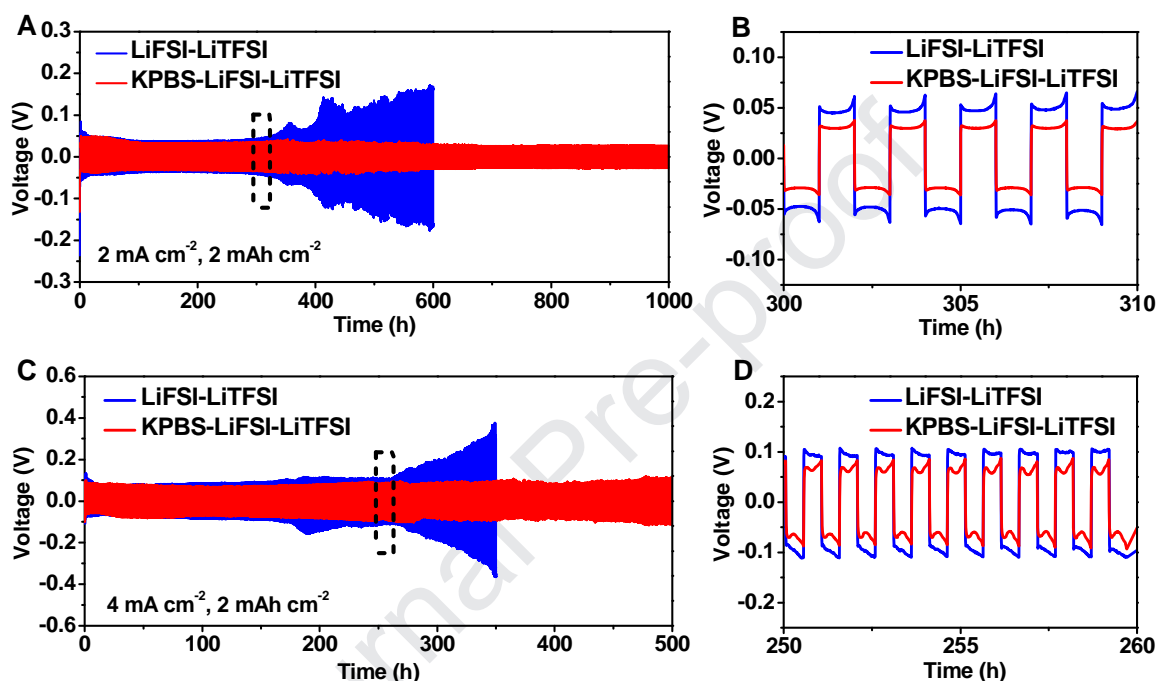


Figure 4 Electrochemical performance of symmetric Li-Li cells. Cycling performance of symmetric Li-Li cells with different electrolytes at a current density of (A) 2 mA cm^{-2} and (C) 4 mA cm^{-2} for a total capacity of 2 mA h cm^{-2} ; Enlarged voltage profiles of symmetric Li-Li cells with different electrolytes at a current density of (B) 2 mA cm^{-2} and (D) 4 mA cm^{-2} for a total capacity of 2 mA h cm^{-2} .

3.3 Li-LFP Full Cells under Relatively Lean Electrolyte Conditions

Electrochemical performance of Li-LFP full cells with two different electrolytes was also evaluated under relatively lean electrolyte conditions to simulate commercial-type cell construction. Initially, Li-LFP full cells were assembled under relatively lean electrolyte ($12.5 \mu\text{L mA h}^{-1}$) and excess Li ($500 \mu\text{m}$ Li metal foil) conditions to capture the effect of electrolyte decomposition on the cycle life of the cells. **Figure 5A, B** shows the

charge/discharge curves of Li-LFP full cells with different electrolytes in the voltage range of 2.5 to 3.8 V. In the KPBS-LiFSI-LiTFSI electrolyte, a large areal capacity of $4.13 \text{ mA h cm}^{-2}$ was obtained at the first cycle with current density of 0.1 mA cm^{-2} , which calls for a large amount of Li plating/stripping. A negligible increase of cell overpotential was observed during cycling process, demonstrating the highly stable Li-electrolyte interface (**Figure 5A**). In the LiFSI-LiTFSI electrolyte, the cell overpotential became larger during the charge/discharge process and the irreversible capacity was higher (**Figure 5B**). Long-term cycling performance of Li-LFP full cells with different electrolytes was also shown in **Figure 5C**. For the KPBS-LiFSI-LiTFSI cell, the capacity remains at 2.9 mA h cm^{-2} after 400 cycles, with a much higher capacity retention than that of the LiFSI-LiTFSI cell (80.0% versus 5.4%). In addition, the KPBS-LiFSI-LiTFSI cell displayed a higher average CE of 99.7% than the LiFSI-LiTFSI cell (99.0%) over 400 cycles, which again can be ascribed to the formation of more stable SEI films on the anode side.

To monitor the Li/electrolyte interface, cycled Li-LFP full cells were disassembled in an Ar-filled glovebox, and the morphology and thickness of Li anodes after 400 cycles were compared by SEM imaging. The LiFSI-LiTFSI cell displayed a loose and porous structure with obvious Li dendrites (**Figure 5D**) with a thickness of $\sim 157 \mu\text{m}$, indicating a large amount of dead Li because of the continuous growth of SEI layers and/or forming dead Li with poor electrochemical connectivity (**Figure 5E**). [24, 55] In sharp contrast (**Figure 5F**), the KPBS-LiFSI-LiTFSI cell exhibited a smooth and more compact SEI structure without Li dendrites. The thickness of surface loose Li was identified to be $48 \mu\text{m}$, suggesting that the consumption of bulk Li and formation of porous dead Li were significantly restricted after 400 cycles (**Figure 5G**).

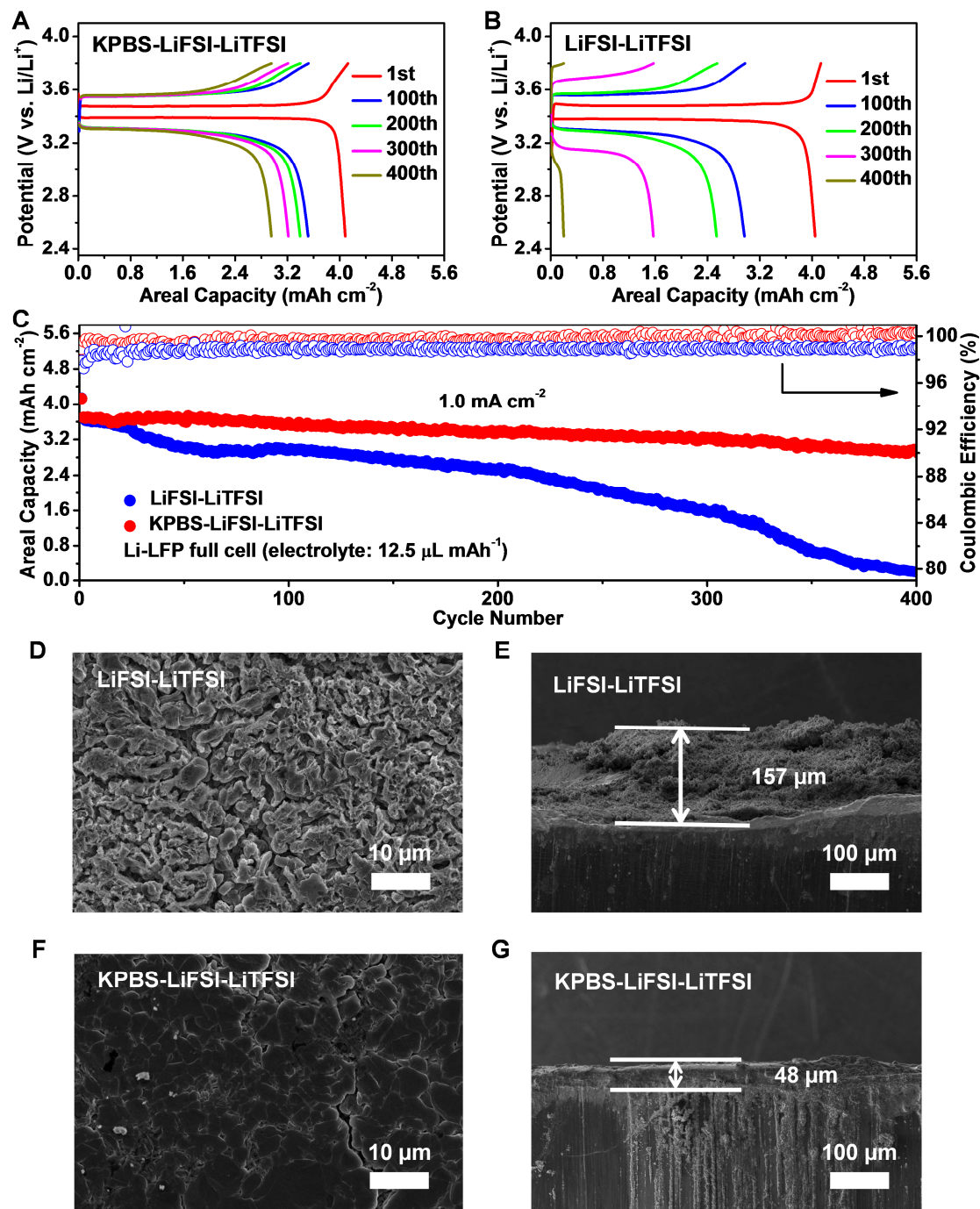


Figure 5 Electrochemical performance and characterization of Li-LFP full cells under relatively lean electrolyte ($12.5 \mu\text{L mA h}^{-1}$) and excess Li (500 μm Li metal foil) conditions. Charge/discharge curves of Li-LFP full cells with different electrolytes: (A) KPBS-LiFSI-LiTFSI, (B) LiFSI-LiTFSI; (C) Cycling performance and CE of Li-LFP full cells with different electrolytes; (D) Top view and (E) Cross-sectional view SEM images of the Li metal anode with LiFSI-LiTFSI electrolyte after 400 cycles; (F) Top view and (G) Cross-sectional view SEM images of the Li metal anode with KPBS-LiFSI-LiTFSI

electrolyte after 400 cycles.

Finally, the Li-LFP full cells were tested with a further reduced electrolyte-to-capacity ratio of $7.5 \mu\text{L mA h}^{-1}$ and limited Li supply from the anode (N/P = 2.4, 1.2 and 0). As shown in **Figure 6A**, with a N/P ratio of 2.4, the KPBS-LiFSI-LiTFSI cell exhibited a large specific capacity of $4.03 \text{ mA h cm}^{-2}$ at the current density of 0.5 mA cm^{-2} in the 1st cycle, which remained stable during 100 cycles with capacity retention of 88.1%. A very high CE of 99.9% was obtained over 100 cycles, highlighting the high reversibility. Although the LiFSI-LiTFSI cell exhibited a similar specific capacity of 4.0 mA h cm^{-2} for the 1st cycle, the capacity decreased quickly to only 2.1 mA h cm^{-2} after 100 cycles, corresponding to a capacity retention of 52.5% and average CE of 98.9%. With a N/P ratio of 1.2, the KPBS-LiFSI-LiTFSI cell still presented high cycling stability with a capacity retention of 80.9%, and average CE at 99.6%, much higher than that of the LiFSI-LiTFSI cell (27.7% and 98.1%, respectively) (**Figure 6B**). Even using Li-free anode (N/P = 0), the KPBS-LiFSI-LiTFSI cell still exhibited significantly improved cycling stability after 100 cycles compared to that of the LiFSI-LiTFSI cell. Furthermore, the average CE of the KPBS-LiFSI-LiTFSI cell still reached 98.7%, much higher than that of the LiFSI-LiTFSI cell (96.6%), further confirming the beneficial role of KPBS in improving SEI stability and Li metal performance (**Figure 6C**). Even compared with the best Li metal full cells reported recently (**Table S1**), our KPBS-LiFSI-LiTFSI cell still stands out in terms of electrolyte amount, N/P ratio, areal capacity and cycling lifetime.

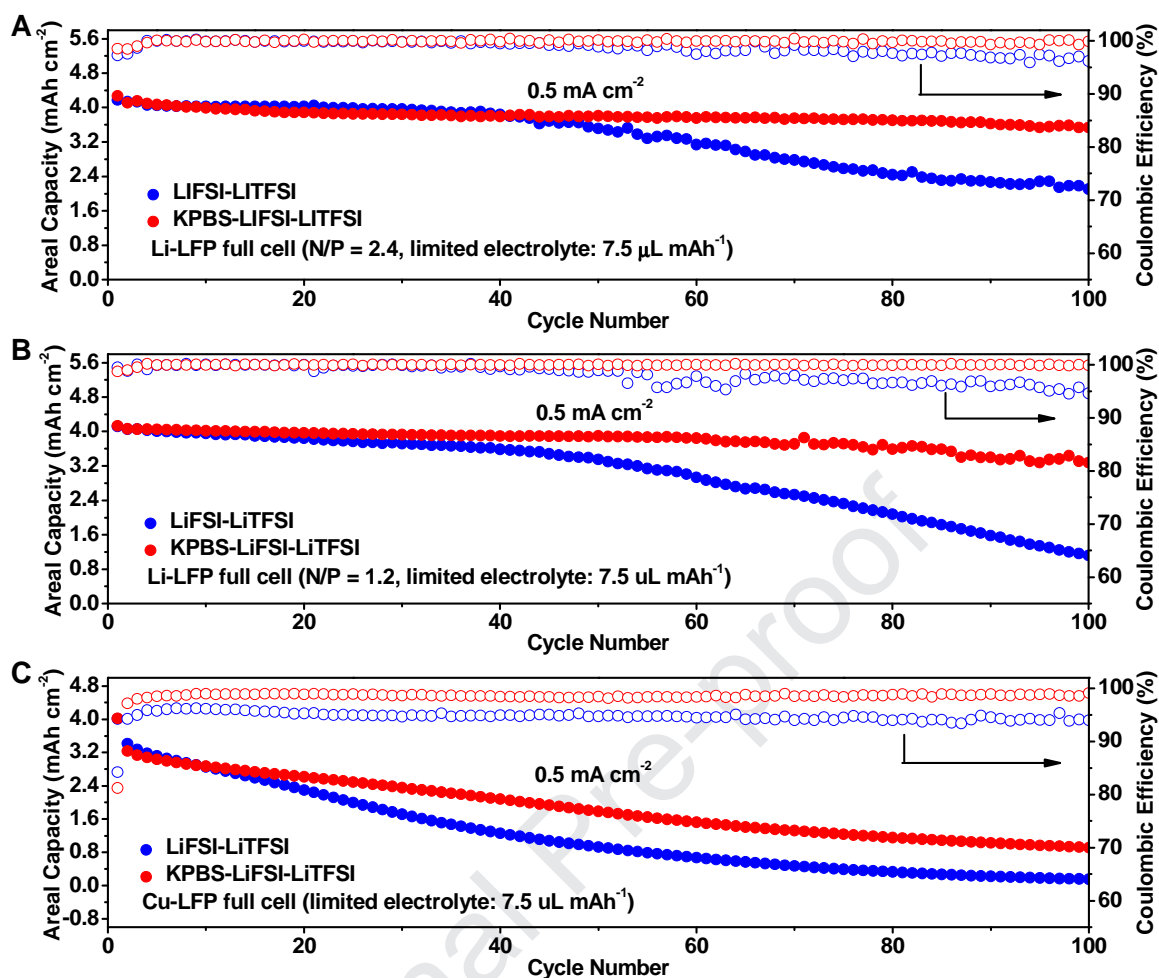


Figure 6 Electrochemical performance of Li-LFP full cells with electrolyte-to-capacity ratio of $7.5 \mu\text{L mA h}^{-1}$. Cycle performance and CE of Li-LFP full cells with different electrolytes under relative lean electrolyte conditions and limited Li supply: (A) $N/P = 2.4$; (B) $N/P = 1.2$; (C) $N/P = 0$.

3.4 Exploring the Mechanisms of the KPBS-LiFSI-LiTFSI Electrolyte

The above results suggest that the addition of KPBS can improve the Li metal deposit morphology and facilitate the formation of more stable LiF-rich SEI layers, leading to higher CE and longer cycling life. The mechanisms of KPBS for stable Li metal anodes may be associated with the favorable reductivity of F-rich PBS^- anions and the electrostatic self-healing effect of K^+ , as detailed below. **Figure 7A** shows the lowest unoccupied molecular orbital (LUMO) and highest occupied molecular orbital (HOMO) levels of three anions (PBS^- , FSI and TFSI) and solvent molecules (DOL and DME) involved in our electrolyte formulation. Both solvent molecules have higher LUMO levels than that of the

three anions, suggesting more favorable reduction of the anions during Li-metal cycling. At the same time, the PBS^- anion has a LUMO level (-1.26 eV) which is between that of the FSI anion (-1.70 eV) and the TFSI anion (-0.91 eV). Such a unique position allows PBS^- to be reduced after FSI but before TFSI, which allows Therefore, PBS^- decomposition can generate fluorine-rich moieties to further enrich LiF in the SEI composition.

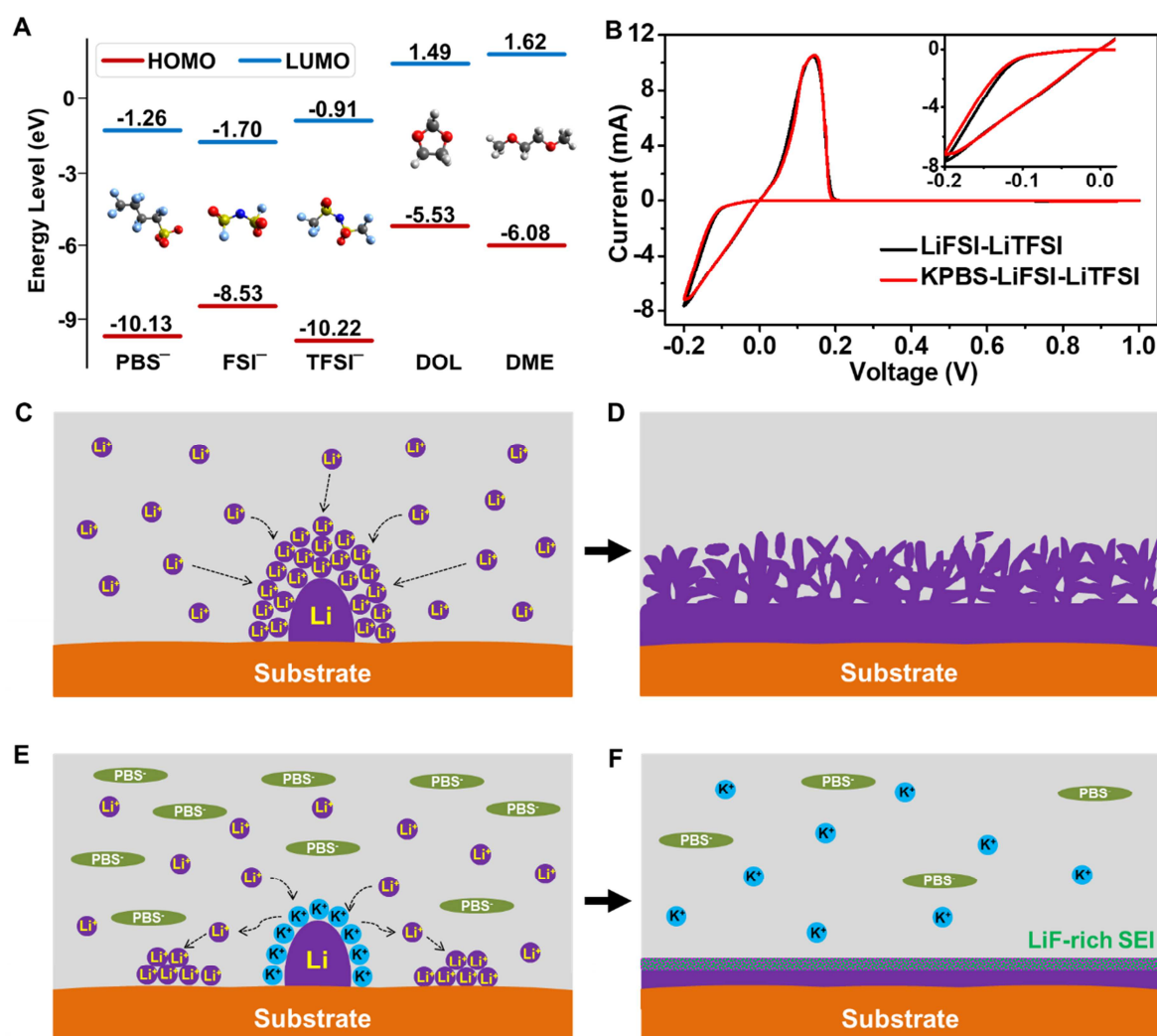


Figure 7 Exploring the mechanism of KPBS-LiFSI-LiTFSI electrolyte. (A) HOMO/LUMO levels of different anions and solvent molecules; (B) CV curves of Li-Cu cells with LiFSI-LiTFSI and KPBS-LiFSI-LiTFSI electrolytes at a scan rate of 0.1 mV s^{-1} . (C-F) The schematic illustration of Li plating/stripping process with two different electrolytes. The KPBS-LiFSI-LiTFSI electrolyte facilitates the formation of more uniform and less porous Li after repeated cycling.

In addition, the presence of K^+ can modulate the Li deposit possibly through a self-healing electrostatic shield mechanism, which was observed by Zhang *et al* using cesium (Cs^+) and rubidium (Rb^+) ions.[56] Achieving a similar electrostatic shield effect using K^+ additive represents a more cost-effective solution. Studies have shown that such shield mechanism depends on an additive cation (M^+) that exhibits a lower reduction potential than that of Li^+ .[56] Thus the effective reduction potentials of Li^+ and K^+ at various concentrations are further calculated and compared in **Table 1**. For a mixed electrolyte with a total Li^+ concentration of 2 M, the Li^+ reduction potential is -3.022V. Therefore, K deposition will not proceed with a K^+ concentration of 0.02 M or below due to a lower reduction potential (-3.032 or below), which makes the electrostatic shield effective. To confirm this, the reduction stability of the different electrolytes was examined by cyclic voltammetry (CV) measurement. CV curves of the two electrolytes displayed similar features in terms of the reduction peak position and current density (**Figure 7B**), suggesting no deposition of K from the electrolyte. XPS results confirm that there are no K 2p peaks in SEI films during different cycles, demonstrating that K^+ is neither co-deposited with Li^+ nor consumed in the cycling process (**Figure S9**).[57] At the same time, energy-dispersive X-ray spectroscopy (EDX) analysis and elemental mapping of the cross-section area of SEI films also shows that there is no K element in SEI layer, further confirming the existence of self-healing electrostatic shield process (**Figure S10**).

Table 1. Summary effective reduction potentials (vs. standard hydrogen electrode or SHE) of Li^+ and K^+ at different concentrations calculated by the Nernst equation.

Cations	E^0 (V)		effective reduction potential (V)		
	1 M	2 M	0.01 M	0.02 M	0.03 M
Li^+	-3.040	-3.022			
K^+	-2.931		-3.049	-3.032	-3.020

For LiFSI-LiTFSI electrolyte without K^+ , initial deposition of Li^+ occurs on the substrate under an applied potential (V_a) smaller than E_{Li/Li^+} and forms some prominent Li metal protrusions owing to various fluctuations originated from the non-uniformity of local

electrolytes and the Cu substrate. More Li^+ will be preferentially deposited around the protrusions instead of on the smooth areas of the anode due to the stronger electrical field of the sharp edges or protrusions,[56] which results in Li dendrites during charge/discharge process (**Figure 7C, 7D**). As for the KPBS-LiFSI-LiTFSI electrolyte, K^+ is adsorbed on protuberant tips due to the stronger electrical field produced by a larger curvature. The adsorbed K^+ with a reduction potential lower than V_a ($E_{\text{k/k}^+} < V_a$) could not be electroplated on the tip.[58] Instead, the K^+ prefers to adsorb around the tips and reject more Li^+ from the tips due to electrostatic charge effect. Hence, Li^+ is deposited in the neighboring areas of the tips, leading to a uniform Li deposition layer (**Figure 7E, 7F**).[56, 57]

The different solvation behavior of K^+ from Li^+ further strengthens the electrostatic shield effect. In the LiFSI-LiTFSI electrolyte, Li^+ is solvated almost exclusively by DOL in the DOL/DME mixture and combines with average three DOL molecules, which dominates the electrolyte decomposition behavior.[59-61] Earlier studies have showed that DOL tends to be electro-reduced to form SEI films consisting of organic moieties ($\text{LiOCH}_2\text{CH}_2\text{OLi}$, $(\text{CH}_2\text{CH}_2\text{OCH}_2\text{OLi})_2$ and $\text{LiO}(\text{CH}_2)_2\text{O}(\text{CH}_2)_3\text{OLi}$) and inorganic species such as Li_2O_2 and Li_2O . [61] These SEI layers are mechanically unstable under large interfacial fluctuations and morphological changes of the Li anode, which continuously consumes a large amount of electrolyte leading to thick SEI films and porous dead Li (**Figure 7D**). With the addition of KPBS, large K^+ cation is solvated by only a single DOL molecule.[62, 63] According to the Marcus reorganization theory as shown below:[64]

$$K = A \exp\left(\frac{-\Delta G'}{k_B T}\right) \quad (1)$$

$$\Delta G' = \frac{\lambda}{4} \left(1 + \frac{\Delta G^\theta}{\lambda}\right)^2 \quad (2)$$

where K is the rate constant of the reorganization reaction, λ the reorganization energy, $\Delta G'$ the free energy of the reorganization reaction and ΔG^θ the standard free energy of reaction (be closed to zero). Computational studies have shown that increasing the number of solvated molecules will increase the reorganization energy of metal ions.[65] Therefore, K^+ with a lower solvation number results in reorganization energy much lower than the solvated Li^+ , which reduces the free energy of reorganization and thus increases the reorganization rate

constant. As a result, the solvated products of K^+ -(DOL) have higher transport rates than the solvated products of Li^+ -(DOL)₃, [66, 67] which enables K^+ to more rapidly occupy the new Li protrusions once they are formed. Together with extra donation of fluorine-moieties from the PBS^- , more uniform and LiF-rich SEI layers are produced (**Figure 7F**).

To study the concentration effect of KPBS, Li-Cu cells with 0.01 and 0.03 M of KPBS were also tested (**Figure S11**). It was observed that cells with 0.02 M KPBS displayed better cycling stability than that with 0.01 M KPBS electrolytes, which indicates that more PBS^- anion decomposition probably leads to more LiF-rich SEI films. The mixed electrolyte with a total K^+ concentration of 0.03 M showed worst cycling stability because the K^+ reduction potential reaches -3.020V, which is higher than that of Li^+ (-3.022V). In order to further confirm the positive effect of K^+ , 0.02 M of lithium nonafluoro-1-butanefluorobutanesulfonate (LPBS) was also used as an additive for the baseline LiFSI-LiTFSI electrolyte to form LPBS-LiFSI-LiTFSI and cycling performance of Li-Cu cells was examined. As shown in **Figure S12**, comparing to LiFSI-LiTFSI cell, the CE and cycling stability of the LPBS-LiFSI-LiTFSI cell were clearly improved. This result suggests the critical role of PBS^- in tuning the LiF-rich SEI composition.

4. Conclusion

In summary, we demonstrated a novel dual function KPBS additive for LiFSI-LiTFSI/ether electrolyte to enable stable Li metal anodes. The cation (K^+) offers an electrostatic shield function and the F-rich anion (PBS^-) exhibits a favorable reductivity for tuning the SEI compositions in the anode. As a result, this additive can effectively promote the formation of a robust LiF-rich SEI during the Li plating/stripping process and drastically slows down the decomposition of organic solvent. These electrolyte properties led to a high CE of 99.1% in Li-Cu cells at current density of 1 mA cm^{-2} with a long cycle life (400 cycles). Even under relatively lean electrolyte (7.5 uL mA h^{-1}) and limited Li supply ($N/P = 1.2$), Li-LFP full cell shows excellent cycling performance of 100 cycles with a high areal capacity of 4.1 mA h cm^{-2} and a high CE of 99.6%. This work provides a simple but effective route towards making Li metal batteries with high capacity and long life through the employment of a novel

salt additive.

Acknowledgements

Z. Chen acknowledges the start-up fund support from UC San Diego. The support provided by China Scholarship Council during a visit of D. D. Wang to University of California San Diego is also acknowledged (No. 201706250088).

Appendix A. Supplementary material

Supporting Information

ORCID

Dongdong Wang: 0000-0002-0391-8242

Zhongqiang Shan: 0000-0001-5316-3186

Ping Liu: 0000-0002-1488-1668

Zheng Chen: 0000-0002-9186-4298

Conflict of Interest

The authors declare no conflict of interest.

References

- [1] D. Lin, Y. Liu, Y. Cui, *Nat. Nanotechnol.*, 12 (2017) 194-206.
- [2] J. Liu, Z. Bao, Y. Cui, E.J. Dufek, J.B. Goodenough, P. Khalifah, Q. Li, B.Y. Liaw, P. Liu, A. Manthiram, *Nat. Energy*, 4 (2019) 180-186.
- [3] S. Chen, C. Niu, H. Lee, Q. Li, L. Yu, W. Xu, J.-G. Zhang, E.J. Dufek, M.S. Whittingham, S. Meng, *Joule*, 3 (2019) 1094-1105.
- [4] J. Zheng, M.H. Engelhard, D. Mei, S. Jiao, B.J. Polzin, J.-G. Zhang, W. Xu, *Nat. Energy*, 2 (2017) 17012.

- [5] K. Yan, Z. Lu, H.-W. Lee, F. Xiong, P.-C. Hsu, Y. Li, J. Zhao, S. Chu, Y. Cui, *Nat. Energy*, 1 (2016) 16010.
- [6] Q. Pang, X. Liang, A. Shyamsunder, L.F. Nazar, *Joule*, 1 (2017) 871-886.
- [7] C. Niu, H. Pan, W. Xu, J. Xiao, J.-G. Zhang, L. Luo, C. Wang, D. Mei, J. Meng, X. Wang, *Nat. Nanotechnol.*, 14 (2019) 594-601.
- [8] C. Yan, X.B. Cheng, Y.X. Yao, X. Shen, B.Q. Li, W.J. Li, R. Zhang, J.Q. Huang, H. Li, Q. Zhang, *Adv. Mater.*, 30 (2018) 1804461.
- [9] M. Wang, Z. Peng, W. Luo, F. Ren, Z. Li, Q. Zhang, H. He, C. Ouyang, D. Wang, *Adv. Energy Mater.*, 9 (2019) 1802912.
- [10] J.I. Lee, M. Shin, D. Hong, S. Park, *Adv. Energy Mater.*, 9 (2019) 1803722.
- [11] C. Fang, X. Wang, Y.S. Meng, *Trends in Chem.*, 1 (2019) 152-158.
- [12] J.W. Choi, D. Aurbach, *Nat. Rev. Mater*, 1 (2016) 16013.
- [13] C.-P. Yang, Y.-X. Yin, S.-F. Zhang, N.-W. Li, Y.-G. Guo, *Nat. Commun.*, 6 (2015) 8058.
- [14] S. Jin, Y. Jiang, H. Ji, Y. Yu, *Adv. Mater.*, 30 (2018) 1802014.
- [15] D. Wang, C. Luan, W. Zhang, X. Liu, L. Sun, Q. Liang, T. Qin, Z. Zhao, Y. Zhou, P. Wang, *Adv. Energy Mater.*, 8 (2018) 1800650.
- [16] N.W. Li, Y.X. Yin, C.P. Yang, Y.G. Guo, *Adv. Mater.*, 28 (2016) 1853-1858.
- [17] J. Zhang, N. Zhao, M. Zhang, Y. Li, P.K. Chu, X. Guo, Z. Di, X. Wang, H. Li, *Nano Energy*, 28 (2016) 447-454.
- [18] D. Lin, D. Zhuo, Y. Liu, Y. Cui, *J. Am. Chem. Soc.*, 138 (2016) 11044-11050.
- [19] C.-C. Su, M. He, R. Amine, Z. Chen, R. Sahore, N.D. Rago, K. Amine, *Energy Storage Mater.*, 17 (2019) 284-292.
- [20] X. Fan, L. Chen, X. Ji, T. Deng, S. Hou, J. Chen, J. Zheng, F. Wang, J. Jiang, K. Xu, *Chem*, 4 (2018) 174-185.
- [21] F. Qiu, X. Li, H. Deng, D. Wang, X. Mu, P. He, H. Zhou, *Adv. Energy Mater.*, 9 (2019) 1803372.
- [22] W. Li, H. Yao, K. Yan, G. Zheng, Z. Liang, Y.-M. Chiang, Y. Cui, *Nat. Commun.*, 6 (2015) 7436.
- [23] R. Miao, J. Yang, X. Feng, H. Jia, J. Wang, Y. Nuli, *J. Power Sources*, 271 (2014) 291-297.

- [24] R. Weber, M. Genovese, A. Louli, S. Hames, C. Martin, I.G. Hill, J. Dahn, *Nat. Energy*, 4 (2019) 683-689.
- [25] S. Jiao, X. Ren, R. Cao, M.H. Engelhard, Y. Liu, D. Hu, D. Mei, J. Zheng, W. Zhao, Q. Li, *Nat. Energy*, 3 (2018) 739-746.
- [26] C.-Z. Zhao, X.-B. Cheng, R. Zhang, H.-J. Peng, J.-Q. Huang, R. Ran, Z.-H. Huang, F. Wei, Q. Zhang, *Energy Storage Mater.*, 3 (2016) 77-84.
- [27] B.D. Adams, E.V. Carino, J.G. Connell, K.S. Han, R. Cao, J. Chen, J. Zheng, Q. Li, K.T. Mueller, W.A. Henderson, *Nano Energy*, 40 (2017) 607-617.
- [28] Y. Liu, D. Lin, Y. Li, G. Chen, A. Pei, O. Nix, Y. Li, Y. Cui, *Nat. Commun.*, 9 (2018) 3656.
- [29] Y. Yuan, F. Wu, Y. Bai, Y. Li, G. Chen, Z. Wang, C. Wu, *Energy Storage Mater.*, 16 (2019) 411-418.
- [30] J. Qian, W.A. Henderson, W. Xu, P. Bhattacharya, M. Engelhard, O. Borodin, J.-G. Zhang, *Nat. Commun.*, 6 (2015) 6362.
- [31] S. Choudhury, L.A. Archer, *Adv. Electron. Mater.*, 2 (2016) 1500246.
- [32] Y. Gao, Z. Yan, J.L. Gray, X. He, D. Wang, T. Chen, Q. Huang, Y.C. Li, H. Wang, S.H. Kim, *Nat. Mater.*, 18 (2019) 384-389.
- [33] P. Xue, S. Liu, X. Shi, C. Sun, C. Lai, Y. Zhou, D. Sui, Y. Chen, J. Liang, *Adv. Mater.*, 30 (2018) 1804165.
- [34] Q. Wang, C. Yang, J. Yang, K. Wu, L. Qi, H. Tang, Z. Zhang, W. Liu, H. Zhou, *Energy Storage Mater.*, 15 (2018) 249-256.
- [35] Y. Ma, Z. Zhou, C. Li, L. Wang, Y. Wang, X. Cheng, P. Zuo, C. Du, H. Huo, Y. Gao, *Energy Storage Mater.*, 11 (2018) 197-204.
- [36] M. Frisch, G. Trucks, H. Schlegel, G. Scuseria, M. Robb, J. Cheeseman, G. Scalmani, V. Barone, B. Mennucci, G. Petersson, *Gaussian Inc.*; Wallingford, CT, (2009).
- [37] A.D. Becke, *J. Chem. Phys.*, 96 (1992) 2155-2160.
- [38] C. Lee, W. Yang, R.G. Parr, *Phys. Rev. B*, 37 (1988) 785-789.
- [39] D.J. Yoo, K.J. Kim, J.W. Choi, *Adv. Energy Mater.*, 8 (2018) 1702744.
- [40] D. Lin, Y. Liu, Y. Li, Y. Li, A. Pei, J. Xie, W. Huang, Y. Cui, *Nat. Chem.*, 11 (2019) 382-389.

- [41] P. Liu, Q. Ma, Z. Fang, J. Ma, Y.-S. Hu, Z.-B. Zhou, H. Li, X.-J. Huang, L.-Q. Chen, *Chinese Physics B*, 25 (2016) 078203.
- [42] J. Hu, G. Long, S. Liu, G. Li, X. Gao, *Chemical Communications*, 50 (2014) 14647-14650.
- [43] C. Yan, X.-B. Cheng, C.-Z. Zhao, J.-Q. Huang, S.-T. Yang, Q. Zhang, *J. Power Sources*, 327 (2016) 212-220.
- [44] N. Dong, G. Yang, H. Luo, H. Xu, Y. Xia, Z. Liu, *J. Power Sources*, 400 (2018) 449-456.
- [45] J.S. Lee, S. Tai Kim, R. Cao, N.S. Choi, M. Liu, K.T. Lee, J. Cho, *Adv. Energy Mater.*, 1 (2011) 34-50.
- [46] S. Eijima, H. Sonoki, M. Matsumoto, S. Taminato, D. Mori, N. Imanishi, *J. Electrochem. Soc.*, 166 (2019) A5421-A5429.
- [47] X. Liang, Q. Pang, I.R. Kochetkov, M.S. Sempere, H. Huang, X. Sun, L.F. Nazar, *Nat. Energy*, 2 (2017) 17119.
- [48] H. Chen, A. Pei, D. Lin, J. Xie, A. Yang, J. Xu, K. Lin, J. Wang, H. Wang, F. Shi, *Adv. Energy Mater.*, 9 (2019) 1900858.
- [49] Y. Gao, D. Wang, Y.C. Li, Z. Yu, T.E. Mallouk, D. Wang, *Angew. Chem. Int. Ed.*, 57 (2018) 13608-13612.
- [50] V.-C. Ho, D.T. Ngo, H.T. Le, R. Verma, H.-S. Kim, C.-N. Park, C.-J. Park, *Electrochim. Acta*, 279 (2018) 213-223.
- [51] K. Xu, *Chem. Rev.*, 114 (2014) 11503-11618.
- [52] X. Fan, L. Chen, O. Borodin, X. Ji, J. Chen, S. Hou, T. Deng, J. Zheng, C. Yang, S.-C. Liou, *Nat. Nanotechnol.*, 13 (2018) 715-722.
- [53] S. Liu, X. Ji, J. Yue, S. Hou, P.-F. Wang, C. Cui, J. Chen, B. Shao, J. Li, F. Han, *J. Am. Chem. Soc.*, 142 (2020) 2438-2447.
- [54] L. Suo, W. Xue, M. Gobet, S.G. Greenbaum, C. Wang, Y. Chen, W. Yang, Y. Li, J. Li, *PNAS*, 115 (2018) 1156-1161.
- [55] Y. Yang, D.M. Davies, Y. Yin, O. Borodin, J.Z. Lee, C. Fang, M. Olguin, Y. Zhang, E.S. Sablina, X. Wang, *Joule*, 3 (2019) 1986-2000.
- [56] F. Ding, W. Xu, G.L. Graff, J. Zhang, M.L. Sushko, X. Chen, Y. Shao, M.H. Engelhard, Z. Nie, J. Xiao, *J. Am. Chem. Soc.*, 135 (2013) 4450-4456.

- [57] Q. Xu, Y. Yang, H. Shao, *Electrochim. Acta*, 212 (2016) 758-766.
- [58] W. Jia, C. Fan, L. Wang, Q. Wang, M. Zhao, A. Zhou, J. Li, *ACS Appl. Mater. Interfaces*, 8 (2016) 15399-15405.
- [59] S.M. Wood, C.H. Pham, R. Rodriguez, S.S. Nathan, A.D. Dolocan, H. Celio, J.P. de Souza, K.C. Klavetter, A. Heller, C.B. Mullins, *ACS Energy Letters*, 1 (2016) 414-419.
- [60] Y. Wang, P.B. Balbuena, *Int. J. Quantum Chem.*, 102 (2005) 724-733.
- [61] Q. Liu, A. Cresce, M. Schroeder, K. Xu, D. Mu, B. Wu, L. Shi, F. Wu, *Energy Storage Mater.*, 17 (2019) 366-373.
- [62] H. Xiang, D. Mei, P. Yan, P. Bhattacharya, S.D. Burton, A. von Wald Cresce, R. Cao, M.H. Engelhard, M.E. Bowden, Z. Zhu, *ACS Appl. Mater. Interfaces*, 7 (2015) 20687-20695.
- [63] M.B. More, E.D. Glendening, D. Ray, D. Feller, P. Armentrout, *J. Phys. Chem.*, 100 (1996) 1605-1614.
- [64] R.A. Marcus, *Angew. Chem. Int. Ed.*, 32 (1993) 1111-1121.
- [65] J.S. Rao, T. Dinadayalane, J. Leszczynski, G.N. Sastry, *J. Phys. Chem. A*, 112 (2008) 12944-12953.
- [66] H. Wang, M. Yoshio, *J. Power Sources*, 195 (2010) 1263-1265.
- [67] I. Skarmoutsos, V. Ponnuchamy, V. Vetere, S. Mossa, *J. Phys. Chem. C*, 119 (2015) 4502-4515.



DEPARTMENT OF NANOENGINEERING
Professor Zheng Chen, Ph.D.
zhengchen@eng.ucsd.edu
(858) 246-0216

MAIL CODE 0448
9500 GILMAN DRIVE
LA JOLLA, CALIFORNIA
92093-0448

Highlights

1. A long-lasting electrolyte additive, potassium nonafluoro-1-butanesulfonate or KPBS, promoting the formation of robust LiF-rich SEI layer on the anode side was discovered;
2. The K^+ cations can offer effective electrostatic shielding that prevents the formation of Li-metal “hot-spots” and the F-rich PBS^- anions with a unique lowest unoccupied molecular orbital (LUMO) level is responsible for the formation of LiF-rich SEI layer;
3. Li-LiFePO₄ full cells with KPBS displayed significantly improved cycling stability with relatively lean electrolyte ($7.5 \mu\text{l mA h}^{-1}$), limited Li supply ($N/P = 1.2$) and high areal capacity (4.1 mA h cm^{-2}) compared with cells without the additive.
4. The electrolyte additive shows promise for practical Li-metal cell applications.

Warm regards,

A handwritten signature in black ink, appearing to read 'zhengchen'.

Zheng Chen
Assistant Professor
Department of NanoEngineering
Program of Materials Science and Engineering
University of California San Diego
Phone: 858-246-0216
Email: zhengchen@eng.ucsd.edu



Dongdong Wang is currently a PhD candidate at School of Chemical Engineering and Technology, Tianjin University. He studied in Prof. Zheng Chen research group at UC San Diego during 2016 and 2019 as a visiting scholar. His research interests focus on the energy storage systems, including Ti-based anode materials, Li metal anode and high-energy cathode materials.



Haodong Liu received his Ph.D. in 2016 from the UC San Diego under Prof. Ying Shirley Meng's guidance, after which he worked as a postdoc research fellow at UC San Diego with Prof. Ping Liu. He is the founder of Electrochemical Society-UCSD Student Chapter (<http://www.ucsdecs.org/>). His recent research topics include the design, synthesis, processing, and operando characterization of advanced electrode materials for Li ion batteries; and novel strategies for high coulombic efficiency dendrite free Li metal anode. Haodong is the author and co-author of more than 50 peer-reviewed journal articles and 3 U.S. patents.



Mingqian Li is currently a graduate student in the Program of Chemical Engineering at UC San Diego in Prof. Zheng Chen group. He received B.E. degree in Chemical Engineering and Technology from University of Hefei University of Technology (HFUT) in 2016. His research interests include the synthesis of nanostructured materials towards battery safety.



Dawei Xia is currently a graduate student in Nanoengineering, UC San Diego in Prof. Zheng Chen group. He received B.E. degree in Renewable Energy Materials and Devices from University of Electronic Science and Technology of China (UESTC) in 2018. His research interests include the synthesis applications of nanostructured materials towards energy storage and conversion.



John Holoubek is a PhD candidate at the University of California, San Diego in the Professor Zheng Chen and Ping Liu research groups. His research focuses on the impact of electrolyte composition and solvation chemistry on next-generation batteries.



Zhi Deng is a Postdoc of NanoEngineering at the UC San Diego in Professor Shyu Ping Ong's group. His research interests focus on understanding thermodynamic and kinetic properties of materials in rechargeable batteries and designing solid-state electrolytes using first-principles methods and atomistic simulations. He studied Materials Science and Engineering at Tsinghua University and obtained his Ph.D. in NanoEngineering from the UC San Diego.



Mingyu Yu received her B.S. degree from the New Energy Science and Engineering department at Xiamen University in 2018, and then received her Master degree from the Materials Science and Engineering department at the UC San Diego in 2020, under the supervision of Prof. Zheng Chen. Her research focuses on the reversible lithium batteries and electrochemical energy storage systems.



Jianhua Tian is a professor at School of Chemical Engineering and Technology, Tianjin University. Her research interests focus on the energy storage and conversion, including lithium ion battery, supercapacitor, solar cells.



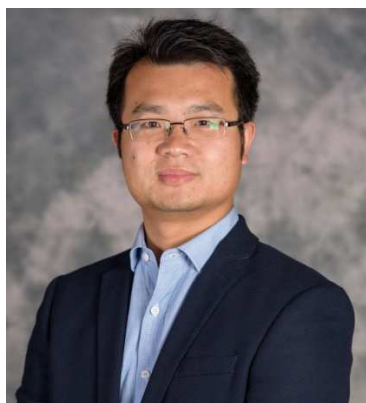
Zhongqiang Shan is a professor at School of Chemical Engineering and Technology, Tianjin University. His research interests focus on the energy storage, including lithium ion battery and lithium sulfur battery



Shyue Ping Ong is an Associate Professor of NanoEngineering at the at the UC San Diego. He leads the Materials Virtual Lab, which focuses on the interdisciplinary application of machine learning and high-throughput first principles computations to accelerate materials design. He is a key developer of the Materials Project and the Python Materials Genomics (pymatgen) materials analysis library. He obtained his PhD from the Massachusetts Institute of Technology in 2011.



Ping Liu is an Associate Professor of NanoEngineering at the UC San Diego. His group develops rechargeable batteries, scalable nanomaterials, and multifunctional electrochemical systems. Prof. Liu was previously a Program Director at ARPA-E, a manager at HRL and a scientist at NREL. He received his Ph.D. in Chemistry from Fudan University in China.



Zheng Chen is an Assistant Professor in NanoEngineering and Program of Chemical Engineering at the UC San Diego. His group focuses on materials and process designs for energy storage and conversion, water desalination and environmental sustainability. Prof. Chen received his B.S. from Tianjin University in 2007 and Ph.D. from UCLA in 2012, both in Chemical Engineering. He did his postdoc research at Stanford University before joining UC San Diego in 2016.

A Long-Lasting Dual-Function Electrolyte Additive for Stable Lithium Metal Batteries under Practical Conditions

Dongdong Wang,^{a,b} Haodong Liu,^a Mingqian Li,^c John Holoubek,^a Zhi Deng,^a Dawei Xia,^a Mingyu Yu,^a Jianhua Tian,^b Zhongqiang Shan,^b Shyue Ping Ong,^a Ping Liu^{a,c,d,e} and Zheng Chen^{a,c,d,e,}*

**Correspondence to: zhengchen@eng.ucsd.edu*

Declarations of interest: none